

Low Energy Excitations and Phase Transitions in the Frustrated Two-Dimensional XY Model

Colin Denniston^{1,2;} and Chao Tang²

¹Department of Physics, Princeton University, Princeton, New Jersey 08544

²NEC Research Institute, 4 Independence Way, Princeton, New Jersey 08540
(March 24, 2022)

We study the critical properties of the two-dimensional (2D) XY model in a transverse magnetic field with filling factors $f = 1/3$ and $2/5$. To obtain a comparison with recent experiments, we investigate the effect of weak quenched bond disorder for $f = 2/5$. A finite-size scaling analysis of extensive Monte Carlo simulations strongly suggests that the critical exponents of the phase transition for $f = 1/3$ and for $f = 2/5$ with disorder are those of the pure 2D Ising model. The relevant low energy excitations are domain walls, and we show that their properties determine the nature of the phase transition.

64.70.Rh, 05.70.Fh, 64.60.Fr, 74.50.+r

I. INTRODUCTION

In this paper we examine the frustrated XY model in two dimensions for two different values of the magnetic field representative of "commensurate states". Experimental realizations of this model in the form of two-dimensional arrays of Josephson junctions and superconducting wire networks [1,3] can and have been constructed and one of the objectives of this work is to understand the results of these experiments. A perpendicular magnetic field induces a finite density of circulating supercurrents, or vortices, within the array. The interplay of two length scales { the mean separation of vortices and the period of the underlying physical array } gives rise to a wide variety of interesting physical phenomena. Many of these effects show up as variations in the properties of the finite-temperature superconducting phase transitions at different fields. In recent experiments on superconducting arrays the critical exponents of a number of these phase transitions have been measured [3], opening the opportunity to do careful comparison of theory and experiment. While we will discuss the model within the context of superconducting networks, the model is also closely related to the physics of adsorbed films on substrates which impose a periodic potential which differs from the preferred period of the adsorbed film. In this work we examine the ground state properties, low energy excitations, and critical properties of the 2D XY model in the densely frustrated regime ($f \rightarrow 0$) for two particular values of the magnetic field. In addition, we investigate the effect of disorder on the ground state and critical properties. This paper elaborates and expands upon our previous results reported in Ref. [4].

The Hamiltonian of the frustrated XY model is

$$H = \sum_{\langle ij \rangle} J_{ij} \cos(\theta_i - \theta_j - A_{ij}); \quad (1)$$

where θ_j is the phase on site j of a square $L_x \times L_y$ lattice and $A_{ij} = (2\pi/\phi_0) \int_i^j \mathbf{A} \cdot d\mathbf{l}$ is the integral of the vector

potential from site i to site j with ϕ_0 being the flux quantum. The directed sum of the \mathbf{A}_{ij} around an elementary plaquette $\mathcal{A}_{ij} = 2\pi f$ where f , measured in the units of ϕ_0 , is the magnetic flux penetrating each plaquette due to the uniformly applied field. We focus here on the cases $f = p/q$ with $p, q = 1, 3$ and $2, 5$.

The ground state vortex pattern for these f is shown in Figure 1(a) [5,6]. The pattern consists of diagonal stripes composed of a single line of vortices for $f = 1/3$ and a double line of vortices for $f = 2/5$. These diagonal lines of vortices can sit on q sub-lattices and, in addition, there are q more states with the stripes going along the opposite diagonal for a total of $2q$ degenerate states. A common speculation for commensurate-incommensurate transitions and the frustrated XY model is that the transition should be in the universality class of the q -state (or $2q$ -state) Potts model. We find that this is not the case because, as discussed below, domain walls between the different states vary considerably in both energetic and entropic factors.

The effect of quenched impurities on phase transitions is an important and fascinating problem. The "Harris criterion" [7] indicates that the addition of (bond) randomness to systems which exhibit second-order transitions in the clean case with a positive specific-heat exponent changes the numerical values of the critical exponents [8]. It has also been shown using phenomenological renormalization-group arguments that the addition of bond randomness to systems undergoing first-order transitions results in a random-field mechanism at any coexistence region which can cause the transition to become continuous [9]. Aizenman and W ehr [10] have shown quite rigorously that in 2D a quenched random field results, quite generally, in the elimination of discontinuities in the order parameter conjugate to the fluctuating field. Most cases where bond disorder has been studied and observed to change the order of the transition are for q -state Potts Models, where for $q = 8$ Chen et al. [11] found through extensive Monte Carlo simulations,

that the first-order transition of the pure model became second-order with the critical exponents being consistent with the universality class of the two-dimensional Ising model. Unlike q -state Potts models with high q , the frustrated XY system is more readily compared to experiments such as recent experimental measurements of critical exponents in superconducting arrays [3].

II. STAIRCASE STATES

The ground states of the Hamiltonian (1) will be among the solutions to the supercurrent conservation equations $\partial_i H = 0$:

$$\sum_{j^0} \sin(\theta_{j^0} - \theta_i - A_{ij^0}) = 0 \quad (2)$$

where j^0 are the nearest neighbors to i . One set of solutions to these equations was found by Halperin [6] by considering the restriction to a quasi-one-dimensional case where one has adjoining staircases of current (see Fig 2(a)). All gauge invariant phase differences $\theta_m = \theta_n - \theta_m - A_{mn}$, within a given staircase are equal and indexing the staircases by m as shown in Fig 2(a) one finds

$$\theta_m = f\theta + 2\pi n_{\text{int}}[f\theta + 2\pi] \quad (3)$$

where n_{int} is the nearest integer function, and $\theta = 0$ for $f = p/q$ with q odd and $\theta = \pi/q$ for q even [6].

The staircase vorticity pattern for $f = 1/3$ and $2/5$ is shown in Fig 1(a) [5,6]. The pattern consists of diagonal stripes composed of a single line of vortices for $f = \frac{1}{3}$ and a double line of vortices for $f = \frac{2}{5}$. (A vortex is a plaquette with unit vorticity occupation, i.e. the phase gains 2π when going around the plaquette.) The stripes shown in Figure 1 can sit on q sub-lattices, which we associate with members of the Z_q group. They can also go along either diagonal, and we associate these two options with members of the Z_2 group. In all, there is a total of $2q$ degenerate states ($f = p/q \notin 1/2$). A common speculation for commensurate-incommensurate transitions and the frustrated XY model is that the transition should be in the universality class of the q -state (or $2q$ -state) Potts model. We find that this is not the case because domain walls between the different states vary considerably in both energetic and entropic factors.

III. DOMAIN WALLS

Figure 1(b)-(e) shows the vorticity pattern for some of the domain walls for $f = 1/3$. The domain walls can be classified into two types. Shift walls involve a shift of the vortex pattern across the wall (such as in Fig 1(b) where the pattern on the right is shifted down by one lattice spacings with respect to the pattern on the left)

but the lines of vortices are still going along the same diagonal. Herringbone walls are walls between states with the vortex stripes going along opposite diagonals. Note that there are q different walls of each type.

These walls also have differing topologies. A herringbone wall is very similar to a domain wall in an Ising model in that it separates two members of a Z_2 group. It cannot branch into other herringbone walls and a 90 degree turn in the wall can be accomplished without changing the vortex pattern, with the caveat that one considers the wall to be composed of sections of length equal to the distance between the diagonal lines of vortices (see Figure 3). Thus, if one only has herringbone walls in the system, the set of possible domain wall configurations is similar to those in an Ising model. Shift walls, on the other hand can branch, both into other shift walls (with the constraint that the sum of the shifts on the walls after the branch be equal to the original shift) and into a pair of herringbone walls, as shown in Figure 3(b). Shift walls also have an associated directionality in the sense that an attempt to make a 90 degree turn in a shift-by- n wall results in the wall changing to a shift-by- $(q-n)$ wall (see Fig. 3(a) for an illustration). Since different shift walls can have quite different energies (see below) one finds bends such as the one shown in Fig. 3(a) are energetically highly unfavorable as it can change a wall with low energy into a wall with a very high energy cost. A more energetically favorable kink in a shift wall can be formed by displacing a mismatched vortex on the wall in a direction parallel to the wall [12]. This displaces a section of the wall one unit cell in the direction perpendicular to the wall (see Figure 3(c)). Typically, one finds only kinks like these of size one or two lattice constants. Larger kinks start to produce long range distortions in the phase field and have higher energy.

In order to calculate the energies of different structures, we solved the equations (2) numerically, using a quasi-Newton method, on lattices with up to 2.3×10^5 sites with constraints fixing the vorticity occupation of each plaquette (see Appendix A). Table I lists the energy per unit length for straight domain walls between the various ground states at zero temperature for $f = 1/3$ and $2/5$. One can see from the table that there is typically one or two walls with considerably lower energy than any of the others. Some of the patterns of energies seen in the table can be understood by counting the number of extra vortices in next or next-next-nearest neighbor plaquettes for the vortices along the wall. For instance, the energy of a $f = 1/3$ shift-by-one wall is about twice that of the standard herringbone wall. Looking at Figure 1(b)-(e) one can see that if you count the number of next-next-nearest neighbor vortices for vortices along each side of the wall, the shift-by-one wall has twice as many as the herringbone. Similarly, walls which place vortices on nearest neighbor sites tend to be of a higher energy, or may not even be stable. While this does give a rough guide to the pattern of energies, it does not allow a strong comparison of walls with differently spaced vortices.

One can see from Figure 3(b) that a shift wall can be viewed as two adjacent, or bound herringbone walls. For $f = 1/3$ the energy of two herringbone walls is less than that of a single shift wall and hence, the shift walls should be unstable to breaking up into herringbone walls. As a result, one expects that in the $f = 1/3$ case if the temperature is high enough for domain walls to enter the system, the herringbone walls should be the only walls present at large length scales. While for $f = 1/3$, herringbone walls are the only stable walls, this is not true for $f = 2/5$. For $f = 2/5$ it is energetically favorable for two herringbone walls to bind and form a shift-by-one or shift-by-three wall. This can lead to more complex domain wall structures and has an important impact on the nature of the finite temperature phase transition. These issues will be addressed in more detail below.

We also numerically calculated the energy of domain walls that are not straight. Figure 5 shows the energy of a square closed domain, formed from herringbone walls, of linear dimension L unit cells in a system of size 120×120 with periodic boundary conditions. We see that to a very good approximation, the energy scales linearly in L . One can, however, work out some corrections to this linear dependence due to the change in the vortex density at the corner of the domain. For instance in Fig. 3(b) the vortices at opposite corners of the square domain have either an extra next-nearest neighbor vortex or a missing next-nearest neighbor. From a distance, this gives a quadrupole moment to the domain. As the 3×3 domain shown in Fig 3(b) is the basic building block of larger domains, one can conclude that larger differently shaped domains will not have a lower moment (i.e. they will be neutral and have no dipole moment). The interaction of two such quadrupole domains at a distance x , large compared to its size L goes like $6J_{eff}(L=x)^4$ (if one assumes an isotropic (which is not really true) interaction of two "corner" charges like $J_{eff} \ln x$). In addition, the self energy of a square quadrupole goes like $2J_{eff} \ln 2 + 2J_{eff} \ln L$.

Figure 4 shows the interaction of some square domains. One sees that the quadrupole correction is measurable and fits the expected functional form quite well, but that the constants J_{eff} do not match what one would expect from an isotropic calculation. In fact, the system is not really equivalent to an isotropic 2D Coulomb gas, in that the direction along the diagonal lines of vortices in the staircase state is not equivalent to the direction perpendicular to the vortex lines. We have also calculated the energies of rectangular domains and some other less regular shapes and they have qualitatively similar (same functional form) behavior.

The next question is whether or not the quadrupole interaction is likely to be relevant. One can use an argument similar to that used to argue for a transition in the unfrustrated XY model. If you consider the interaction free energy contribution of the quadrupole interaction, it should contain the energetic part $A=r^4$ and an entropic part $B T \ln(r^2)$ from counting the quadrupoles

to have a separation less than r (One could do a more accurate calculation of the entropy but it will still have a $\ln r$ dependence). At the distances at which the $A=r^4$ form is valid, the $\ln r$ term wins all the time (at finite T) and hence one can argue that the quadrupole interactions should not be relevant.

IV. SPIN WAVES

At low enough temperature, domains should be small, and one is tempted to expand the energy about the ground state configuration. In this treatment, the periodic character of the angles is neglected, but the existence of long range order in the vortex lattice partly justifies this method. The model is replaced by a so-called spin wave approximation which involves expanding the Hamiltonian to 2nd order in ϕ_{ij} , where $\phi_{ij} = \phi_{ij}^{(0)} + \phi_{ij}$ and $\phi_{ij}^{(0)}$ is a ground state configuration:

$$H = H^{(0)} + \sum_{ij} \frac{\partial H}{\partial \phi_{ij}} \phi_{ij}^{(0)} + \frac{1}{2} \sum_{ij} \sum_{kl} \frac{\partial^2 H}{\partial \phi_{kl} \partial \phi_{ij}} \phi_{kl}^{(0)} \phi_{ij} \quad (4)$$

By definition, $(\partial H / \partial \phi_{ij})^{(0)} = 0$ and we just have a quadratic form. The free energy per site associated with (4) is

$$F = -\frac{1}{\beta} \ln Z_{sw} = -\frac{1}{\beta} \ln \int \prod_i d\phi_i \exp \left[-\frac{1}{2} \sum_{x,x^0} \phi_x J_{xx^0} \phi_{x^0} + i \sum_{x,x^0} \phi_x \phi_{x^0} \right] \quad (5)$$

where J is the Jacobian matrix, $J_{xx^0} = \partial^2 H / \partial \phi_x \partial \phi_{x^0}$. The spin wave correlation function is

$$G_{sw}(x_1; x_2) = \langle \exp[i(\phi_{x_1} - \phi_{x_2})] \rangle = Z_{sw}^{-1} \int \prod_x d\phi_x \exp \left[-\frac{1}{2} \sum_{x,x^0} \phi_x J_{xx^0} \phi_{x^0} + i(\phi_{x_1} - \phi_{x_2}) \right] = \exp \left[-\frac{1}{2} X(x_1; x_2)^T J^{-1} X(x_1; x_2) \right]; \quad (6)$$

where $X(x_1; x_2)$ is a vector with $+1$ and -1 in positions x_1 and x_2 respectively and zeros everywhere else.

For the unfrustrated case [13] J is just the discretization of the Laplacian operator (i.e. ∇^2), where $\nabla^2 = \partial^2/\partial x^2 + \partial^2/\partial y^2$ and the partial derivatives are replaced with a finite-difference formula $\partial^2/\partial x^2 \approx (x_{i+1}y_i - 2x_iy_i + x_{i-1}y_i)/a^2$, and a is the lattice constant). As a result, $\frac{1}{2}X(x;x^0)^T J^{-1} X(x;x^0)$ can be approximated by the Green's function for the Poisson equation,

$$g(r) = \frac{1}{2} \ln \frac{r}{r_0};$$

where $r_0 = a/(2\pi e)$, a is the lattice spacing and $\gamma = 0.577216$ is Euler's constant. This yields

$$G_{sw}(x_1; x_2) = \exp(-\ln(x_1 - x_2)/r_0) = (x_1 - x_2)^{-1/2} \quad (7)$$

So the correlation function of the spin wave fluctuations decreases according to a power law behavior. This algebraic decay of the spin wave correlation function is broken by the unbinding of vortex-antivortex pairs at the Kosterlitz-Thouless transition [13].

In the general frustrated case, J is not a discrete Laplacian. The question is, do we get something similar? The $1/r^4$ interaction of the domains studied in the previous section suggests that we do. Figure 6 shows $\frac{1}{2}X(x;x^0)^T J^{-1} X(x;x^0)$ for $f = 1/3$ along a slice in the x -direction in a finite size system with periodic boundary conditions along the direction of the slice. The envelope of this curve is well described by the sum of two logarithmic functions, $\ln x + \ln(L - x)$ (where the second term comes from the periodic boundary conditions). In addition to this logarithmic part, there is a periodic oscillation, coinciding with the underlying vortex lattice. In addition to this obvious oscillation, the phase of the oscillation depends on the initial x (The correlation function is not just a function of $(x - x^0)$). The effect of this initial x dependent phase at long distances should not be important. However, distortions centered on nearby sites, and between rows of vortices can partially cancel due to this phase difference. There is also an anisotropy between the directions perpendicular and parallel to the diagonal lines of vortices. This anisotropy can, however, be removed in a continuum picture by rescaling the coordinates.

This modified lattice "Green's" function also has an impact on vortex interactions. The presence of the logarithmic part ensures that the overall flux balancing ($f = \ln_i$ where n_i is the vortex occupation of plaquette i) is maintained. However the vortex interaction energy should contain an oscillating component coinciding with the underlying vortex lattice. The effect of such a component is not entirely clear, especially as the amplitude of the oscillation does not decay away at large distances. Conventional wisdom would suggest that as long as we still have the logarithmic interaction of vortices, they should still undergo a Kosterlitz-Thouless type of

unbinding transition and an associated jump in the helicity modulus [13]. As we shall see in the next section, it is not entirely clear whether or not this actually happens. It might be interesting to try to go through and derive the Kosterlitz recursion relations with the oscillations as some sort of perturbation to see if it is relevant, although it seems unlikely to do anything but renormalize the core energies.

$$V \cdot f = 1/3$$

The fluxoid pattern for the two lowest energy walls at $f = \frac{1}{3}$ was shown in Figure 1 (b) and (d). One can see from Figure 3 (b) that a shift wall can be viewed as two adjacent, or bound herringbone walls. For $f = \frac{1}{3}$ the energy of two herringbone walls is less than that of a single shift wall and hence, the shift walls are unstable and break up into herringbone walls. As a result, we confine our discussion of the $f = \frac{1}{3}$ case to the herringbone walls as other walls should not be present at large length scales. The energy cost for dividing an $L \times L$ lattice into two domains separated by a solid-on-solid (SOS) wall stretching from one side of the system to the other is

$$H_{single\ fzg} = bL + b \sum_k z_k z_{k+1} \quad (8)$$

The height variables z_k take on integer values ($b = 3$ is the shortest length segment). The partition function, $Z = \sum_{\{z_k\}} \exp(-H/T)$ can be evaluated either by the transfer matrix method or recursively (see Appendix B) [14]. The interfacial free energy per column is $F = T \ln \langle e^{b/T} \tanh(b/(2T)) \rangle$: The zero crossing of F gives an estimate of the critical temperature. Plugging in the values for the $f = \frac{1}{3}$ herringbone wall gives $T_c = 0.19J$, in remarkable agreement with the value $T_c = 0.22J$ found in the Monte Carlo simulations described below.

Being similar to Ising walls, herringbone walls cannot branch into other herringbone walls, thus the set of possible domain wall configurations is similar to those in an Ising model. We label the fraction of the system in state $(s; j)$ as $m_{s;j}$, where $s = 1$ denotes the member of Z_2 , and $j = 1; 2; 3$ denotes the member of Z_3 . Below the transition, one state $(s; i)$ spans the system. On this state sit fluctuating domains, bounded by herringbone walls, of each of the states $(s; 1); (s; 2);$ and $(s; 3)$ in equal numbers; so the Z_3 symmetry is broken for the $(s; j)$ states, but not for the $(-s; j)$ states. As the transition is approached from below, the domains occupied by the $(-s; j)$ states grow, with smaller domains of the $(s; j)$ states within them. At the transition, the Z_2 symmetry between the s states is restored and, as a result, the Z_3 symmetry for the $(s; j)$ states is also restored.

The Monte Carlo simulations used a heat bath algorithm with system sizes of 20×96 . We computed between 10^7 and 3×10^7 Monte Carlo steps (complete

lattice updates) with most of the data taken close to T_c . Data from different temperatures was combined and analyzed using histogram techniques [15] (see Appendix C).

If the largest fraction of the system is in state $(s; i)$, then we have three Ising order parameters, $M_j = \langle m_{s; i} m_{s; j} \rangle = \langle m_{s; i} + m_{s; j} \rangle$; $j = 1, 2, 3$. On average, these M_j are the same so we just take the average as M . To calculate the $m_{s; i}$, we examine the Fourier transform of the vortex density ρ_k at the reciprocal lattice vectors $k = \frac{2\pi}{3}(1; 1)$ of the ground state vortex lattices. Starting from the definition of the Fourier transform, and using the vortex states given above, one finds

$$\frac{\rho_k}{g} = m_{1;1} + m_{1;2} e^{i2\pi/3} + m_{1;3} e^{-i2\pi/3}; \quad (9)$$

where g is the modulus in the ground state. In practice, ρ_k is reduced by small short-lived regions which don't quite match any of the six states. Since this effect is the same for all states, it cancels when calculating M . Using the real and imaginary parts of ρ_k in addition to $\sum_j m_{1;j}$, calculated from the direct vortex lattice as in [16], we can find the v independent $m_{1;j}$.

In addition to the energy and order parameter, several other quantities were calculated from the Monte Carlo data using the corresponding fluctuation-dissipation relations:

$$\begin{aligned} \frac{C}{k_B} &= \frac{K^2}{L^2} (\langle E^2 \rangle - \langle E \rangle^2); \\ &= K L^2 (\langle M^2 \rangle - \langle M \rangle^2); \\ \frac{\partial \ln M}{\partial K} &= \frac{\langle M^2 \rangle - \langle M \rangle^2}{\langle M \rangle^2} \langle E \rangle; \end{aligned} \quad (10)$$

where $K = J/k_B T$. In addition to the discrete order parameter, we also followed the helicity modulus defined by $Y_{x,y} = \partial^2 F / \partial^2 j = 0$, where F is the free energy density and j is a twist in the boundary condition along the x or y direction. The helicity modulus also follows a fluctuation-dissipation relation which is used in calculating it from the data:

$$\begin{aligned} Y_x &= \frac{1}{L^2} \sum_{hr;r^0i}^* X [(r - r^0) \cdot \hat{x}]^2 \cos(\mathbf{r} - \mathbf{r}^0 \cdot \mathbf{A}_{x;r^0i}) \\ &\quad + \frac{J^2}{L^2} \sum_{hr;r^0i}^* 2 X [(r - r^0) \cdot \hat{x}] \sin(\mathbf{r} - \mathbf{r}^0 \cdot \mathbf{A}_{x;r^0i}) \\ &\quad + \frac{J^2}{L^2} \sum_{hr;r^0i}^* X [(r - r^0) \cdot \hat{x}] \sin(\mathbf{r} - \mathbf{r}^0 \cdot \mathbf{A}_{x;r^0i}) \end{aligned} \quad (11)$$

where $hr;r^0i$ denotes nearest neighbor pairs.

To determine the critical exponents for the transition we make use of finite size scaling [17]. Following standard arguments, one assumes that for a second-order transition, the singular part of the free energy, $F(t; h)$, near the

transition is dominated by a term that changes under a change of scale according to the ansatz

$$F(t; h) = L^{\frac{d}{\nu}} F(t L^{1/\nu}; h L^{\frac{1}{\nu}})$$

where $t = (T - T_c)/T_c$ and h is an applied field which couples to the order parameter M (so h is not the true magnetic field here). From this, one can derive the scaling form of the order parameter, specific heat, susceptibility, etc. using the standard relations, $M = \partial F / \partial h$, $C = -T \partial^2 F / \partial t^2$, $\chi = \partial M / \partial h$, etc. If one takes the special case $h = 0$; $\chi \sim |t|^{-\gamma}$ one can relate γ 's to the standard exponents for the specific heat, for the order parameter, and for the susceptibility as $\nu = 1/(2 - \beta)$, $\beta = (1 - \gamma)/2$ and $\gamma + 2 - \beta = 2$. If one takes the case $h = 0$ and $\chi \sim L^{-(2-\beta)}$, where β is the exponent for the divergence of the correlation length, one obtains the relations for finite size scaling:

$$\begin{aligned} M^n &= L^{-\frac{d}{\nu}} M_n(x_t); \\ C &= L^{\frac{d}{\nu}} C(x_t); \\ &= L^{\frac{d}{\nu}} X(x_t); \end{aligned} \quad (12)$$

where $x_t = t L^{1/\nu}$ is the temperature scaling variable. Using relations 12 one can also derive [11,18]

$$\begin{aligned} \frac{\partial \ln M}{\partial T} &= L^{-\frac{1}{\nu}} D(x_t); \\ \frac{\partial \ln C}{\partial T} &= L^{1-\frac{1}{\nu}} Q(x_t); \end{aligned} \quad (13)$$

For a finite lattice the peak in, for example the specific heat, scales with system size like $C_{max} / L^{\frac{d}{\nu}}$ and occurs at the temperature where the scaling function $C(x_t)$ is maximum so that

$$\frac{C(x_t)}{dx_t} \Big|_{x_t=x_t^*} = 0;$$

This defines the finite-lattice transition temperature $T_c(L)$ by the condition $x_t = x_t^*$ so that $T_c(L) = T_c + T_c x_t^* L^{-1/\nu}$. In general the finite-lattice transition temperature calculated from different quantities differs slightly but extrapolates to the same T_c in the limit of large L .

A very accurate way of locating the transition temperature is by using Binder's cumulant [19],

$$U = 1 - \frac{\langle M^4 \rangle}{3 \langle M^2 \rangle^2};$$

shown in Figure 7. For system sizes large enough to obey finite-size scaling, this quantity is size independent at the critical point. From Fig. 7 we find $T_c = 0.2185(6)J$. T_c can also be determined from the scaling equation for the temperature at the peak of thermodynamic derivatives such as the susceptibility, $T_c(L) = T_c + a L^{-1/\nu}$. We find these other methods give T_c in agreement with that from U .

Finite size scaling [17] at T_c applied to $\ln M = \theta K$ gives $\theta = 1.011 \pm 0.029$, and to the susceptibility gives $\theta = 1.758 \pm 0.013$, and to M gives $\theta = 0.14 \pm 0.02$. These exponents are determined from the slopes of the lines shown in Fig. 9 which plots the values of these quantities at the critical point as function of L . These exponents are in excellent agreement with the Ising values $\theta = 1$, $\theta = \frac{7}{4}$, and $\theta = \frac{1}{8}$. Fig. 8 shows the collapse of the raw data onto the scaling function (inset) for $\theta = 1$.

Two previous examinations of the $f = \frac{1}{3}$ case [12,20] suggested a continuous transition but did not measure critical exponents. Lee and Lee [16] claim to find separate, closely spaced transitions, for the breaking of Z_2 and Z_3 . One explanation for their conflicting results comes from the small system sizes ($L \leq 42$) used in their analysis. Below the transition, if the dominant state is $(s; i)$, in small systems you often do not see all three of the $(s; j)$ states in the system at the same time. Figure 10 illustrates this effect. The minimum of $(k_+; k_-)$ is a measure of the Z_3 symmetry breaking for the $(s; j)$ states and this goes to zero as $L \rightarrow \infty$. The finite value of $\min(k_+; k_-)$ for small L can give the impression of separate transitions for small systems (If a measured parameter contains a contribution from $\min(k_+; k_-)$ its derivatives can have a double peaked structure from the derivative of $\min(k_+; k_-)$). One must take care in the choice of order parameter to ensure that this contribution is not biasing the results. For example we found that the derivative of the Ising order parameter used in [16], $M^0 = m_1 + m_2 + m_3 - m_4 - m_5 - m_6$ has a double peaked structure for intermediate lattice sizes that does not completely go away until $L = 96$. This makes M^0 an unsuitable choice of order parameter for finite-size scaling. This is also the probable cause of the presence of a shoulder in the specific heat at intermediate system sizes [16]. For larger L , we see this shoulder merge with the main peak and for $L = 84$ and 96 it is no longer clearly discernible (see Fig. 11).

The helicity modulus Y is the quantity most closely related to experimental measurements [13]. For $f \neq 0$, the scaling of the I - V curves found in experiments is consistent with domain wall activation processes [3]. The theory of Nelson and Kosterlitz for the $f = 0$ case predicts that Y should come down in a characteristic square-root cusp and then jump with a universal value, $2k_B T_{KT} = \dots$. However, we find an exceptionally good fit (Fig. 12) of our data to $Y = Y_0 = L^{-\theta} = M^{-\theta} ((T - T_c)L^{1-\theta})$ with $\theta = 1$, $\theta = \frac{1}{8}$, and $Y_0 = 0$, which is the scaling form of M . Clearly, Y is affected strongly by fluctuations in M and attempting to fit scaling relations for the $f = 0$ case [16] without taking this into account seems questionable. We see two possible interpretations of our result. The first is that Y only receives contributions from the ordered part of the lattice. So comparisons with the $f = 0$ case should examine $Y_m = Y/M$. $Y_m = 0.58$ at the transition implying a larger than universal jump. Alternatively, one can say that although Y is brought down by fluctuations in M , it should still jump when it crosses the universal

value, $2k_B T = \dots$. Extrapolating the observed behavior of Y gives $Y_{L \rightarrow \infty} = a(T - T_c)^j$. This crosses the value of the universal jump at $T_{KT} = T_c + 10^{-6}$. Although we do not see evidence for a jump, a difference in transition temperatures of 10^{-6} would not lead to any observable effects for the system sizes studied here.

$$VI. f = 2/5$$

While for $f = \frac{1}{3}$, herringbone walls are the only stable walls, this is not true for $f = \frac{2}{5}$. For $f = \frac{2}{5}$ it is energetically favorable for two herringbone walls to bind and form a shift-by-one or shift-by-three wall. Binding does, however, have an entropic cost. To see if these walls are bound we consider the following model for two SOS walls:

$$H_d(f; z_g) = \sum_k [f(2b + u_k z_k; 0) + b \sum_k z_k - z_{k+1}] + (2b + u_? z_k; 0) z_k + V_r(f; z_g)g \quad (14)$$

z_k is the separation of the walls ($z_k \geq 0$), k is the number of vertical steps the two walls take in the same direction in the k 'th column ($-1 < k < 1$). u_k and $u_?$ are the binding energies parallel and perpendicular to the wall. At this stage we take $V_r = 0$. The solution to such a model is discussed in Appendix B. A ground state eigenvector $(z) = e^{-z/l}$, where $l = \dots$ is the localization length, or typical distance separating the lines, characterizes the bound state of the two lines. $l = 0$ defines the unbinding transition at T_b . For the cases of interest, one finds $T_b = 0.398J$ for the shift-by-one walls and $T_b = 0.442J$ for the shift-by-three walls. In addition, the free energy for these walls crosses zero before they unbind. Hence, at the transition, defined by the point at which the walls enter the system, we expect a branching domain wall structure similar to the $q = 5$ Potts models where a first order phase transition occurs. Technically, this is a mean field argument for the interfaces but, since the interfaces are extended objects it should give a reasonable picture of the order of T_b for the interfaces and T_c .

In their Monte Carlo simulations, Li and Teitel [21] observed hysteresis of the internal energy when the temperature was cycled around the transition and used this as an argument for a first order transition at $f = \frac{2}{5}$. The most direct indication of a first order transition is the presence of a free energy barrier between the ordered and disordered states which diverges as the system size increases [22]. The free energy as a function of energy is obtained using $F_L(E) = -\ln P_L(E)$ where $P_L(E)$ is the probability distribution for the energy generated by Monte Carlo simulation of a $L \times L$ system. Figure 13 shows the growth in this barrier as the system size increases from $L = 20$ to 80 giving clear evidence for the first order nature of the transition.

Since there is no diverging characteristic length to which the linear dimension L could be compared at a

first order transition, one finds that it is simply the volume L^d that controls the size effects [23]. One thus finds

$$C_{max} \propto L^d$$

for a first-order transition. Figure 15 shows the specific heat as a function of L^2 for the $f = 2/5$ clean system. The linear fit (solid line) clearly shows the expected first-order scaling behavior. Similar behavior can be seen in the susceptibility as shown in the Figure. From the positions of the peaks as a function of L we obtain $T_c = 0.2127(2)J$.

VII.D DISORDER AND THE $f = 2/5$ PHASE TRANSITION

We now consider the effects of disorder on the $f = 2/5$ phase transition. Taking the couplings in the Hamiltonian (1) as $J_{ij} = J(1 + \epsilon_{ij})$, the ϵ_{ij} are chosen randomly from a Gaussian distribution with a standard deviation

. Due to variations of the phase differences across the bonds, a specific realization of random bonds may favor a certain sub-lattice for the ground state, creating an effective random field. To quantify the effect, we placed the dimer configuration of the ground states down on 10 000 separate realizations of the disorder and allowed the continuous degrees of freedom (the phases) to relax and minimize the energy. We find that the changes in energy from the $\epsilon = 0$ case to a Gaussian distribution with mean $0.5^2 L^2$ and standard deviation L . The difference in energy between states which were degenerate in the clean system is the measure of the random field. This difference centers on zero and has a standard deviation of $0.75 L$ for two states related by a shift and $0.57 L$ for two states with vortex rows along opposite diagonals. The effect of random fields on discrete degrees of freedom in 2D is marginal [24]. For $D > 2$ there is a critical randomness above which random fields cause the formation of domains in the ground state of size ℓ_f .

Aizenman and Wehr have shown that this critical randomness is zero in 2D [10]. Yet, their result does not preclude the possibility that ℓ_f is so large as to be unobservable in a finite sized sample. Indeed, experiments on superconducting arrays have found apparent phase transitions, including scaling behavior [3] in sample sizes of order 1000–10000. In our simulations with disorder at

0.1, all system had a low temperature state with the order parameter approaching unity. We will, therefore, ignore the effects of random fields for $\epsilon \leq 0.1$ assuming that ℓ_f is larger than the sample size.

At any coexistence point of the clean system, random bonds result in different regions of the system experiencing average couplings slightly above or below the critical coupling. As a result, at any given temperature the system will predominantly prefer either the ordered or disordered state wiping out the coexistence region and leaving only a continuous transition [24,9,10]. It has been

conjectured [11] that critical random Potts models are equivalent to Ising models. Kardar et al. [25] suggested a possible mechanism for this effect. Their position space renormalization group approximation suggests that the probability of loop formation in the fractal interface of the clean system vanishes marginally at a transition dominated by random bonds. The interface may have some finite width due to a froth of bubbles of different phases, but under renormalization a linear critical interface is obtained and, hence, an Ising transition appears.

The dimer configurations from our simulations suggest that for large enough disorder, ($\epsilon > \epsilon_f$) the interface is really linear, not just in the renormalized sense. ϵ_f can be estimated by placing a random potential V_r in Eq. 14. Ignoring the terms involving ϵ_k , one obtains the model for wetting in the presence of disorder, solved by Kardar [26] in the continuum limit. He obtained a new length scale due to randomness,

$$l = \epsilon / 2T^3 = K^{-2}$$

where K is the renormalized stiffness related to the interfacial free energy γ by $K = \gamma(0) + \frac{1}{2} \int \gamma(q) dq = \frac{1}{2} \int \gamma(q) dq$ where γ is a small tilt angle of the interface. For an Ising-like interface $K = T \sinh \phi = T \ln \coth(\phi = (2T))$ [14]. The unbinding transition is lowered and is now defined by the condition $l = 0$. As T_0 decreases, it eventually hits the transition temperature for the first order phase transition observed in the clean system. At this point any branched domain wall structure is unstable. This is just the last step in a process in which the effective linear interface becomes narrower as disorder increases. In the vicinity of this "narrow" (mean-field) unbinding, the Ising-type behavior of the system should be readily visible at any length scale.

We have done a Monte Carlo analysis with bond disorder values of $\epsilon = 0.05$ and 0.1 . Since we are dealing with quenched disorder, we are interested in averaged quantities; for instance the free energy is

$$F = -k_B T [\ln Z]_{av} \quad (15)$$

where the square brackets indicate an average over different realizations of disorder. Since most quantities of interest involve derivatives of the free energy, to calculate the average value of a thermodynamic quantity, we first calculate it for a given realization of the disorder and then do a configurational average over 10 to 15 realizations for $\epsilon = 0.1$ and seven realizations for $\epsilon = 0.05$. Figure 14 shows the free energy barrier for $f = 2/5$ as a function of system size in the for $\epsilon = 0.05$, and 0.1 . For $\epsilon = 0.05$, the barrier first grows with system size and then levels off. At $\epsilon = 0.1$ the free energy barriers are essentially zero, indicating a continuous transition and that the system sizes are large enough to apply finite size scaling. Here, we follow the finite-size scaling methods used in [11].

Figure 16 shows the peak values of $\partial \ln M / \partial K$ and $\partial \ln M / \partial T$ as a function of L . The slopes of these plots give

$1/\nu = 1.05(12)$ and $\beta/\nu = 1.70(12)$. A similar analysis of $\partial M/\partial K$ gives $(1/\nu) = 0.94(10)$ [4]. As in the $f = 1/3$ case, the helicity modulus appears to track the order parameter M . Within errors, these exponents are what one would expect from an Ising model. Experiments at $f = 2/5$ [3] also found a continuous transition and measured the critical exponents $\beta = 0.9(5)$ and the dynamic critical exponent $z = 2.0(5)$, consistent with an Ising transition.

VIII. CONCLUSIONS

In conclusion, we find that the nature and universality class of the phase transitions are quite sensitive to the proximity of the binding transition for the lowest energy domain walls. For $f = 1/3$ the lowest energy walls are never bound and the transition is Ising-like. For $f = 2/5$ domain walls can lower their free energy by binding to each other, resulting in a first order phase transition. Disorder weakens this binding and changes the transition to be continuous and Ising-like. These results are consistent with the continuous phase transition and critical exponents observed experimentally for $f = 2/5$ [3].

We thank M. Aizenman, P. Chandra, J. M. Kosterlitz, X. S. Ling, and D. Huse and for useful discussions.

APPENDIX A: CONSTRAINED OPTIMIZATION FOR VORTEX LATTICES

Minima of the Hamiltonian (1) satisfy Equations (2). However, these equations are written in terms of the θ_j variables and the locations of the vortices does not enter explicitly. This is quite inconvenient as one finds that the zero temperature energies of the system are almost entirely dictated by the vortex structure. By this we mean that given the position of all the vortices, the phases appear to be uniquely determined (up to an overall constant) by the minimization conditions. This can be made more explicit by working with the gauge invariant phase differences

$$\begin{aligned} \theta_{ij} - \theta_{i,j-1} &= \frac{2}{0} \sum_{(i,j)}^{Z(i,j)} A \, dl; \\ \theta_{ij} - \theta_{i-1,j} &= \frac{2}{0} \sum_{(i,j)}^{Z(i-1,j)} A \, dl; \end{aligned} \quad (A1)$$

where θ_{ij} is the phase on the site at row i column j of the lattice. This introduces an extra variable per site (instead of just θ_{ij} now we have θ_{ij} and $\theta_{i,j-1}$) and a compensating constraint that

$$\theta_{ij} - \theta_{i-1,j} + \theta_{ij} - \theta_{i,j-1} - 2\pi(f - n_{ij}) = 0: \quad (A2)$$

That is to say, the sum of the gauge invariant phase differences around any plaquette must equal the magnetic

flux through the plaquette $2\pi f$, plus an integer multiple n_{ij} of 2π . If the gauge invariant phase differences are restricted to a range of 2π such as $[-\pi; \pi)$ then n_{ij} measures the vortex occupancy of the plaquette and is typically 0 or ± 1 with the sign depending on the sign of f .

One then rewrites Equations (2) in terms of the gauge invariant phase differences to get

$$\sin \theta_{ij} - \sin \theta_{i,j+1} + \sin \theta_{i+1,j} - \sin \theta_{ij} = 0: \quad (A3)$$

If disorder is added, the random couplings should be included here. These, in addition to Eq.'s (A2) give $2MN$ equations (for a lattice of $M \times N$ unit cells) for the $2MN$ unknown gauge invariant phase differences. The vortex pattern $f n_{ij}$ is now an input and stays fixed. When periodic boundary conditions are imposed one finds that two of these equations are not independent. Two more convenient conditions to impose closure are

$$\begin{aligned} \sum_{j=1}^N \sin \theta_{N,j} - I_c &= 0; \\ \sum_{i=1}^M \sin \theta_{i,1} - I_r &= 0; \end{aligned} \quad (A4)$$

where I_c is the net current flowing down the columns of the lattice and I_r is the net current flowing along the rows. In all cases found, the lowest energy state corresponded to $I_{rc} = 0$.

The above equations can now be organized into the form $F(f, \theta_{ij}; \theta_{i,j-1}) = 0$ as

$$\begin{aligned} F_1 &= \sum_{i=1}^M \sin \theta_{i,1} - I_r; \\ F_{2M(i-1)+2j-1} &= \theta_{ij} - \theta_{i-1,j} \\ &\quad + \theta_{ij} - \theta_{i,j-1} - 2\pi(f - n_{ij}); \\ F_{2M(i-1)+2j} &= \sin \theta_{ij} - \sin \theta_{i,j+1} \\ &\quad + \sin \theta_{i+1,j} - \sin \theta_{ij}; \\ F_{2MN} &= \sum_{j=1}^N \sin \theta_{N,j} - I_c; \end{aligned} \quad (A5)$$

If we define x to have elements $x_{2M(i-1)+2j-1} = \theta_{ij}$ and $x_{2M(i-1)+2j} = \theta_{ij} - \theta_{i,j-1}$ ($i = 1 \dots N$ and $j = 1 \dots M$) then the solution to (A5) can be found using Newton's method which involves iteratively solving

$$J \, x = -F \quad (A6)$$

and updating x ,

$$x_{\text{new}} = x_{\text{old}} + \Delta x; \quad (A7)$$

where the Jacobian $J_{ij} = \partial F_i / \partial x_j$.

The set of equations (A6) can be very large (we solved system s with up to $2 \times 3 \times 10^6$ sites which means Eq. (A6) represents about half a million simultaneous equations).

In addition, we need to solve these systems very fast, especially when disorder is added and averages over tens of thousands of solutions are needed. This is made possible by the special form of the Jacobian matrix:

$$J = \begin{array}{c} \begin{array}{ccccc} 2 & & & & 3 \\ 6 & & & & 7 \\ \vdots & & & & \vdots \\ \vdots & & & & \vdots \\ 4 & & & & 5 \end{array} \end{array} \quad (\text{A } 8)$$

where the dots represent the non-zero elements. We see that J is very nearly band diagonal. In fact J can be written as

$$J = A + U \quad \bar{V} \quad (\text{A } 9)$$

where A is the band diagonal part of J (the same three matrix diagonal blocks as J) and U and V are $N \times 2M$ matrices (as opposed to $2M \times 2M$). I should point out here that the method described below has a speed that is proportional to $N M^2$ so that the axes of the lattice should always be chosen so that $M \ll N$ for efficient operation. U and V have the form

$$U^T = \begin{array}{c} \begin{array}{ccccc} 2 & & & & 3 \\ 4 & 1 & 0 & 1 & 0 \\ & & & & \\ & & & & \\ & & & & \\ & & & & \end{array} \end{array} \quad \begin{array}{c} 3 \\ 5 \\ 3 \\ 5 \end{array} ;$$

$$V^T = \begin{array}{c} \begin{array}{ccccc} 2 & & & & 3 \\ 4 & 1 & 0 & 1 & 0 \\ & & & & \\ & & & & \\ & & & & \\ & & & & \end{array} \end{array} \quad \begin{array}{c} 3 \\ 5 \end{array} ; \quad (\text{A } 10)$$

The first two blocks of U and V^T have the nonzero elements indicated and the remaining blocks of U are from the first block column of J and the remaining blocks of V are from the first block row of J .

The solution of a band diagonal system $A x = b$ is considerably simpler than solving a general linear system of $2M \times N$ equations. Not only that, but the LU factorization of A has the same storage requirements as A which can be stored in a packed storage scheme holding only the central nonzero band. In order to solve our slightly more general problem we make use of the Woodbury formula [27]:

$$J^{-1} = (A + U \quad \bar{V})^{-1} = A^{-1}$$

$$A^{-1} U \quad (1 + \bar{V}^T A^{-1} U)^{-1} \quad \bar{V}^T A^{-1} : \quad (\text{A } 11)$$

Since storage of A^{-1} is not practical (the inverse does not preserve the band structure of the matrix), we must make use of (A 11) in the following way, as described in [27]: To solve the linear equation

$$(A + U \quad \bar{V}) x = F \quad (\text{A } 12)$$

first solve the $2M + 1$ auxiliary problems

$$A z = U ; \quad (\text{A } 13)$$

and

$$A y = F : \quad (\text{A } 14)$$

This can be done by LU factorizing A once and then using the factorization to solve all the systems simultaneously. Routines from LAPACK [28] can make this very fast and efficient. Next, do the $2M \times 2M$ matrix inversion

$$H = (1 + \bar{V}^T z)^{-1} : \quad (\text{A } 15)$$

In terms of these quantities, the solution is given by

$$x = y - z H (\bar{V}^T y) : \quad (\text{A } 16)$$

In order to start Newton's method, one needs a good initial guess. This is provided by patching together the staircase state solutions described in section II. In addition, care must be taken to ensure that the gauge invariant phase differences do not wander out of $[-\pi; \pi]$. There are a number of options one can use if a phase difference wanders out of range. One is to just pin the solution at π . This is not a great solution as this is not really a minimum of the unconstrained Hamiltonian. Another solution is to just add or subtract 2π and continue iterating Newton's method. This can cause a jump in the errors on one of the equations which may result in a large change in x at the next step which may or may not be beneficial. Another solution is to replace the phase difference with the value on the other branch of the arcsin function on $[-\pi; \pi]$. This causes no change in the error on the current conservation equations and produces a smaller change in the corresponding Eq. (A 2). Many of these problems can often be avoided by taking a step in the Newton direction but with smaller length, especially in the initial stages, using a dynamic step length algorithm similar to those described in [27].

APPENDIX B: SOLID ON SOLID MODELS

A good review of interface models is given in [14]. Here we briefly discuss the cases relevant to our situation. The SOS model of an interface ignores overhangs and bubbles

and configurations can be described in terms of integer-valued height variables whose values are measured from the $T = 0$ position of the interface (see Figure 17). The energy cost for dividing an $L \times L$ lattice into two domains separated by a solid-on-solid (SOS) wall stretching from one side of the system to the other is

$$H_{\text{single fzg}} = bL + b \sum_k j_k - z_{k-1} j \quad (\text{B1})$$

The height variables z_k take on integer values (b is the shortest length segment). The partition function, $Z = \sum_{\{z_k\}} \exp(-H/T)$ can be easily evaluated by change of variables, $i = z_i - z_{i-1}$ so that

$$Z = \sum_{k=1}^Y e^{-b \sum_{k=1}^X i_k} e^{-b \sum_{k=1}^X i_k};$$

where $[r; r]$ is the allowed values of i_k . In the unrestricted case $r = 1$, the interfacial free energy per column is $F = T \ln [e^{-b} \tanh(b/(2T))]$; The zero crossing of F gives an estimate of the critical temperature. In the case of the two-dimensional Ising model this zero crossing gives the exact critical temperature. This is somewhat fortuitous, but nevertheless useful.

In the continuum limit, the problem of two interfaces can usually be broken down into a center of mass part and an independent part involving the separation of the two interfaces. We would prefer, however, to work with a discrete model with parameters input from the energy calculations of the appropriate bent domain walls. We were unable to find the solution to such a model in the literature, so we present one here. Questions that we are interested in are whether or not the two interfaces are bound and whether or not unbinding occurs before or after the free energy of the walls becomes negative. To answer these questions we consider the following model for two SOS walls shown in Figure 18:

$$H_{\text{double f}}; z_g = \sum_k f(2b + u_k z_{k,0}) + b \sum_k j_k - z_{k-1} j + (2b + u_? z_{k,0}) k g; \quad (\text{B2})$$

where z_k is the separation of the walls ($z_k \geq 0$), and k is the number of vertical steps the two walls take in the same direction in the k 'th column ($-1 < k < 1$). u_k and $u_?$ are the binding energies parallel and perpendicular to the wall.

The partition function is

$$Z = \sum_{\{z_k\}} e^{-b \sum_k j_k - z_{k-1} j} e^{-(2b + u_k z_{k,0})} f(1 + j_k - z_{k-1} j) + \sum_{k \in 0} e^{-(2b + u_? z_{k,0}) j} k j g \quad (\text{B3})$$

The $(1 + j_k - z_{k-1} j)$ comes from the fact that for $k = 0$ there are $j_k - z_{k-1} j + 1$ ways to divide the change

$j_k - z_{k-1} j$ between the two lines. Summing over k leaves the partition function in the form of a transfer matrix:

$$Z = \sum_{\{z_k\}} e^{-b \sum_k j_k - z_{k-1} j} f_{z_k,0} (j_k - z_{k-1} j) + \coth[(b + u_? = 2)] e^{-(2b + u_k)} + (1 - z_{k,0}) (j_k - z_{k-1} j + \coth b) e^{2b g} = \sum_{\{z_k\}} T_{z_k, z_{k-1}} \quad (\text{B4})$$

Unfortunately, we were unable to solve the general case analytically. However, restricting $z_k - z_{k-1}$ to 0 or 1, we can derive the eigenvalues and eigenvectors of the matrix \hat{T} explicitly. A ground state eigenvector $(z) = e^{-z}$, where $1 =$ is the localization length, or typical distance separating the lines, characterizes the bound state of the two lines. (z) is found by first finding the eigenvalue (from the defining equation $\hat{T}(z) = (z)$) for $z > 0$. z is then obtained from the eigenvalue equation for $z = 0$. This gives e as the solution to the quadratic equation,

$$(1 + \coth b) e^2 + e^{-b} \coth b - e^{-u_k} (1 + 2e^{-(2b + u_?)}) e^{-1} + 1 + \coth b - 2e^{-u_k} (1 + e^{-(2b + u_?)}) = 0; \quad (\text{B5})$$

$= 0$ defines the unbinding transition at T_b . The more general case, $j_k - z_{k-1} j < N$ with N a large number (typically about 1000), can be easily solved numerically and is not that different from the restricted case discussed above. The values quoted in the text are from such a numerical calculation.

APPENDIX C: MONTE CARLO SIMULATION OF CONTINUOUS SPIN SYSTEMS

A reasonable introduction to Monte Carlo techniques is given in [29]. However, some of the implementation techniques suggested in this book are out of date and should be taken with a lump of salt. Most simulations of frustrated spin systems described in the literature appear to have used a rather poor updating scheme leading to very long autocorrelation times. We use a heat bath scheme described below which seems to be a couple of order of magnitude faster than these standard schemes near the critical point. This is not to say that other heat bath schemes have not been used, it is just that such works almost never describe any details of how this is done, a problem we shall try to rectify here. To make efficient use of the data generated in a Monte Carlo simulation one should make use of the histogram techniques of References [15,22].

1. Sampling

Formally, the task of statistical mechanics is to compute from the model Hamiltonian H the desired average properties,

$$\langle A(f_{ij}g) \rangle = \frac{1}{Z} \int df_{ij}g A(f_{ij}g) \exp[-H(f_{ij}g)/T]; \quad (C1)$$

where states are weighted with the normalized Boltzmann distribution

$$p(f_{ij}g) = \frac{1}{Z} \exp[-H(f_{ij}g)/T]; \quad (C2)$$

While this gives a formally exact description of the probability distribution, we are not really interested in such detailed information, nor is it possible to carry out the integrations in the high-dimensional space required in the thermodynamic limit. The dimension of the space can be reduced somewhat by making use of finite size scaling to extrapolate from small systems ($L < 100$) to the thermodynamic limit. Even for these smaller L , it is still not possible to numerically integrate the system based on any sort of discretization scheme. One instead uses Monte Carlo integration which is simply to pick N sets of $f_{ij}g$ randomly distributed according to (C2) and then

$$\langle A(f_{ij}g) \rangle = \frac{1}{N} \sum_{l=1}^N A(f_{ij}g_l); \quad (C3)$$

If the $f_{ij}g_l$ are independent and $A(f_{ij}g)$ is distributed in a Gaussian distribution with variance σ^2 then the error in $\langle A \rangle$ calculated in this manner is σ/\sqrt{N} .

In practice, the knowledge of how to pick independent random numbers distributed according to (C2) is quite close to knowing how to solve the problem exactly. In general, we must give up on the idea of independent random numbers and instead construct a Markov process where each state $f_{ij}g_{l+1}$ is constructed from a previous state $f_{ij}g_l$ via a suitable transition probability $W(f_{ij}g_l \rightarrow f_{ij}g_{l+1})$. A sufficient condition for the distribution function $P(f_{ij}g)$ of states generated to converge to (C2) in the limit $N \rightarrow \infty$, is for the transition probability to satisfy detailed balance:

$$\frac{W(f_{ij}g_l \rightarrow f_{ij}g_{l+1})}{W(f_{ij}g_{l+1} \rightarrow f_{ij}g_l)} = \exp\left[-\frac{H(f_{ij}g_{l+1}) - H(f_{ij}g_l)}{T}\right]; \quad (C4)$$

where $H = H(f_{ij}g_{l+1}) - H(f_{ij}g_l)$. Note that equation (C4) must be satisfied for all possible moves $l \rightarrow l+1$ in order to be ergodic.

This still leaves many choices for the move. Ideally, one would like to change many degrees of freedom simultaneously, unfortunately in the absence of any cluster routines for frustrated systems, one is left with single

site updating moves. (Alternatively one can simulate a Langevin equation to change all degrees of freedom simultaneously, but by a small amount. Even Langevin dynamics are not unique, and the dynamics which are supposed to be appropriate for superconducting arrays [12] was found to have longer autocorrelation times than the Monte Carlo method we ended up using.) One particularly poor, but popular, method of updating continuous degrees of freedom involves picking a new ij completely at random, or in an interval about its previous value, and then accepting or rejecting the move based on whether another random number is above or below $\exp[-\frac{H}{T}]$. This can give extremely long autocorrelation times, and leads to a high number of rejected moves in the low temperature state. One would have to apply this same step numerous times to the same spin just to equilibrate it with its nearest neighbors.

An ideal single site updating step would pick ij according to the conditional Boltzmann probability $p(ij)$ for ij given the knowledge of the neighboring spins $f_{ij-1}; f_{i+1,j}; f_{i,j-1}; f_{i,j+1}$. For our frustrated XY model this is

$$\begin{aligned} p(ij) &= \frac{1}{C} \exp\left(\cos(\theta_{ij+1} - \theta_{ij} + A_{ij}^{ij+1}) \right. \\ &\quad + \cos(\theta_{ij-1} - \theta_{ij} + A_{ij}^{ij-1}) \\ &\quad + \cos(\theta_{i+1,j} - \theta_{i,j} + A_{i+1,j}^{ij}) \\ &\quad \left. + \cos(\theta_{i-1,j} - \theta_{i,j} + A_{i-1,j}^{ij})\right) \\ &= \frac{1}{I_0\left(\frac{h}{T}\right)} \exp\left[\frac{h}{T} \cos(\theta_{ij})\right]; \end{aligned} \quad (C5)$$

where

$$\begin{aligned} h &= \sqrt{x^2 + y^2}; \\ &= \arctan(x/y); \\ x &= \sin(\theta_{ij+1} + A_{ij}^{ij+1}) + \sin(\theta_{ij-1} + A_{ij}^{ij-1}) \\ &\quad + \sin(\theta_{i+1,j} - A_{i+1,j}^{ij}) + \sin(\theta_{i-1,j} - A_{i-1,j}^{ij}); \\ y &= \cos(\theta_{ij+1} + A_{ij}^{ij+1}) + \cos(\theta_{ij-1} + A_{ij}^{ij-1}) \\ &\quad + \cos(\theta_{i+1,j} - A_{i+1,j}^{ij}) + \cos(\theta_{i-1,j} - A_{i-1,j}^{ij}); \end{aligned} \quad (C6)$$

and $I_0(x)$ is the zeroth order modified Bessel function.

An excellent reference for the next step can be found in [30]. In order to generate a distribution of θ with $p(\theta)$ given by (C5), one first generates a uniform deviate x (independent uniformly distributed random number between 0 and 1) and makes use of the fundamental transformation law of probabilities, which simply tells us

$$p(\theta)d\theta = p(x)dx; \quad (C7)$$

So we need to solve

$$\frac{dx}{d\theta} = p(\theta); \quad (C8)$$

The solution of this is $x = F(\theta)$, where $F(\theta)$ is the indefinite integral of $p(\theta)$. The desired transformation which

takes a uniform deviate into one distributed as $p(\cdot)$ is therefore

$$(x) = F^{-1}(x) \quad (C 9)$$

where F^{-1} is the inverse function to F . This process is illustrated in Figure 19.

Unfortunately, F (and F^{-1}) can only be computed numerically. In order to implement the method we used look-up tables and interpolation. On systems where integer operations are much faster than floating point operations, things can be speeded up considerably by discretizing the i_j (for instance one can take the integers 0 to 524288 to correspond to 0 to 2) and then storing all possible values of the sinusoidal functions that can occur (all 524288 values). This requires some storage capacity (about 64 M byte for our implementation) but this should not be onerous for any machine that one would consider doing such simulations on. One should note that some machines can compute trigonometric functions in only a few clock cycles and therefore it may be faster than a look-up call to memory. The resulting code took about twice as long per Monte Carlo step (MCS) to run as the simple "pick at random and then reject" method, but this loss is more than compensated for by the orders of magnitude improvement in correlation times. There is still considerable freedom in the order in which subsequent lattice sites are selected. Naively, one would think that, as long as all sites are visited on some pseudo regular basis, that the order is unimportant. While this is true in the sense that the order is unimportant for eventually reaching equilibrium, the order can have a huge impact on how fast you get there. The slowest (in the sense of long correlation times) method is to select sites at random. One can significantly reduce (by a factor of up to about L depending on temperature) correlation times by going through the lattice in typewriter fashion or a mixture of random and typewriter ordering. However, one must go through in different directions (alternate left-right-up-down with up-down-left-right etc.) in order for the correlation times to be isotropic (i.e. have the same correlation time for say Y measured in both the x and y direction). To ensure the accuracy of the implementation, the code was tested against published results for the $f = 0$ and $f = 1/2$ cases.

2. Error Analysis

Suppose we make N successive observations A_i , $i = 1; \dots; N$, of a quantity A in our simulation. If the distribution of the fluctuations in A is Gaussian (this is not true for all the parameters measured), then the expectation value of the square of the statistical error, which in this case is the variance, is

$$h(A^2)_i = \frac{1}{N} \sum_{i=1}^N (A_i - \bar{A})^2$$

$$\begin{aligned} &= \frac{1}{N^2} \sum_{i=1}^N h(A_i - \bar{A})^2 \\ &+ \frac{2}{N^2} \sum_{i=1}^N \sum_{j=1}^N (A_i - \bar{A})(A_j - \bar{A}) \\ &= \frac{1}{N} \sum_{i=1}^N (A_i^2 - \bar{A}^2) \\ &+ \frac{2}{N} \sum_{i=1}^N \sum_{j=1}^N (A_i - \bar{A})(A_j - \bar{A}) \end{aligned} \quad (C 10)$$

The autocorrelation function for A is defined as

$$A(t) = \frac{h(A_0 A_i - \bar{A}^2)}{h(A^2)_i - \bar{A}^2} \quad (C 11)$$

where we associate the time t with step i . Note that $A(0) = 1$ and $A(t)$ decays to zero as $t \rightarrow \infty$. The autocorrelation time τ_A is defined as

$$\tau_A = \sum_{i=1}^{\infty} A(t) \quad (C 12)$$

For an exponential relaxation, τ_A is the relaxation time, so that for times $t \gg \tau_A$, $A(t)$ is very small. If $N \gg \tau_A$ we can, therefore neglect the term involving τ_A in Eq.(C 10) and one obtains

$$h(A^2)_i = \frac{1}{N} \sum_{i=1}^N (A_i^2 - \bar{A}^2) (1 + 2\tau_A) \quad (C 13)$$

Thus, our N correlated measurements are equivalent to $N = (1 + 2\tau_A)$ independent measurements, something that must be taken into account when calculating errors.

The concept of self-averaging (or lack of) is extremely important in correctly estimating errors from Monte Carlo simulations with disorder. Suppose we measure A and calculate its statistical error using $h(A^2)_i$ from Eq.(C 13). If $h(A^2)_i$ reduces to zero if $L \rightarrow \infty$ (and $N = (1 + 2\tau_A)$ fixed) we say A exhibits self-averaging. If, on the other hand, $h(A^2)_i$ reaches an L -independent nonzero limit, we say A exhibits a lack of self-averaging. Random systems exhibit a lack of self-averaging near the critical point [31]. In fact, the distribution of most quantities (over realizations of disorder) is not even Gaussian, making the use of $h(A^2)_i$ as a measure of the statistical error somewhat questionable.

In calculating errors we make use of, among other things, the bootstrap resampling technique described in [32] and more compactly in [27]. From the set of data D_0 produced by our Monte Carlo simulation we calculate a set x_0 of parameters such as the energy, order parameter, etc. Due to the random sampling, D_0 is not a unique realization of the true parameters x_{true} . With different initial conditions or other slight variations we could have

measured any of an infinite number of other realizations D_1, D_2, \dots . Although the x_0 is not the true one x_{true} , we assume that the shape of the probability distribution $x_i - x_0$ is the same, or very nearly the same, as the shape of the probability distribution $x_i - x_{\text{true}}$. This is not an assumption that x_0 and x_{true} are the same, it is just assuming that the way in which random errors enter the simulation does not vary rapidly as a function of x_{true} , so that x_0 can serve as a reasonable surrogate.

Suppose we have in some way obtained a set of equivalent realizations of our data. For each realization D_j we calculate the parameters x_j in the same way as we obtained x_0 from D_0 . Each simulated measured parameter set yields a point $x_j - x_0$. If we simulate enough data sets we can map out the desired probability distribution for the parameter space. As mentioned above, this distribution of parameters is not necessarily Gaussian so we require some means of defining what we mean by the statistical error. We take the statistical error to be width of the confidence region that contains 68% of the data (i.e. the confidence region is defined by the interval x where, given the set of realizations of the parameter x , 68% of the x_j lie between x_0 and $x_0 + \dots$). In this way, if our distribution is Gaussian, our definition of the error is just the standard deviation, as one would want for compatibility with the standard case.

It only remains to explain how we obtain "a set of equivalent realizations of our data". The bootstrap method [32] used the actual data set D_0 , with its $n = N/(1 + 2A)$ "independent" data points, to generate any number of synthetic data sets D_j^S , with n data points. The procedure is simply to draw n data points at a time with replacement from the set D_0 . For the bond disordered systems this includes bootstrap resampling of the set of realizations of bond disorder, as well as bootstrap resampling of the data from an individual realization of disorder. The basic idea behind the bootstrap is that the actual data set, viewed as a probability distribution, is the best available estimator of the underlying probability distribution.

Present Address: Dept. of Physics, Theoretical Physics,
University of Oxford, 1 Keble Road, Oxford OX1 3NP.

- [1] For a general review, see Physica B 152, 1-302 (1988).
- [2] C. Denniston and C. Tang, Phys. Rev. Lett. 75, 3930 (1995).
- [3] X.S. Ling, et. al., Phys. Rev. Lett. 76, 2989 (1996); M. Higgins, P. Chaikin, S. Bhattacharya, to be published.
- [4] C. Denniston and C. Tang, Phys. Rev. Lett. 79, 451 (1997).
- [5] S. Teitel and C. Jayaprakash, Phys. Rev. Lett. 51, 1999 (1983).
- [6] T.C. Halsey, Phys. Rev. B 31, 5728 (1984); T.C. Halsey,

- J. Phys. C 18, 2437 (1985).
- [7] A.B. Harris, J. Phys. C 7, 1671 (1974).
- [8] Numerical studies of impure Ising models are reviewed in: W. Selke, in "Computer Simulation Studies in Condensed Matter Physics, IV", ed. by D.P. Landau, K. Mon, and H.-B. Schüttler (Springer-Verlag, Heidelberg); results for impure Baxter and Baxter-Wu models are given in: D. Matthews-Morgan, D.P. Landau, and R.H. Swendsen, Phys. Rev. Lett. 53, 679 (1984); M.A. Novontny and D.P. Landau, Phys. Rev. B 24, 1468 (1981).
- [9] K. Hui and A.N. Berker, Phys. Rev. Lett. 62, 2507 (1989).
- [10] M. Aizenman and J. Wehr, Phys. Rev. Lett. 62, 2503 (1989).
- [11] S. Chen, A.M. Ferrenberg, and D.P. Landau, Phys. Rev. Lett. 69, 1213 (1992).
- [12] F. Fab, A.R. Bishop and P.S. Lomdahl, Phys. Rev. B 41, 10983 (1990).
- [13] J.M. Kosterlitz and D. Thouless, J. Phys. C 6, 1181 (1973); D.R. Nelson and J.M. Kosterlitz, Phys. Rev. Lett. 39, 1201 (1977); B.I. Halperin and D.R. Nelson, J. Low Temp. Phys. 36, 1165 (1979).
- [14] G. Forgacs, R. Lipowsky and Th. Nieuwenhuizen, in Phase Transitions and Critical Phenomena, Vol. 14, ed. C.Domb and J.L. Lebowitz (Academic Press, New York, 1991); and references therein.
- [15] A.M. Ferrenberg and R.H. Swendsen, Phys. Rev. Lett. 61, 2635 (1988); *ibid.* 63, 1195 (1989).
- [16] S. Lee and K.-C. Lee, Phys. Rev. B 52, 6706 (1995).
- [17] see Finite Size Scaling and Numerical Simulation of Statistical Systems, ed. V. Privman (World Scientific, Singapore, 1990); and references therein.
- [18] A.M. Ferrenberg and D.P. Landau, Phys. Rev. B 44, 5081 (1991).
- [19] K. Binder, Phys. Rev. Lett. 47, 693 (1981).
- [20] G. Grest, Phys. Rev. B 39, 9267 (1989).
- [21] Y.H. Li and S. Teitel, Phys. Rev. Lett. 65, 2595 (1990).
- [22] J. Lee and J.M. Kosterlitz, Phys. Rev. Lett. 65, 137 (1990).
- [23] Y. Imry, Phys. Rev. B 21, 2042 (1980); M.E. Fisher and A.N. Berker, Phys. Rev. B 26, 2507 (1982); J.L. Cardy and M.P. Nightingale, Phys. Rev. B 27, 4256 (1983); V. Privman and M.E. Fisher, J. Stat. Phys. 33, 385 (1983).
- [24] Y. Imry and S. Ma, Phys. Rev. Lett. 35, 1399 (1975).
- [25] M. Kardar et al., Phys. Rev. E 52, R1269 (1995).
- [26] M. Kardar, Phys. Rev. Lett. 55, 2235 (1985).
- [27] W.H. Press et. al., Numerical Recipes, 2nd Edition (Cambridge Univ. Press, 1992).
- [28] <http://csep1.phy.ornl.gov/comellproceedings/tutorials/Xnetlib/xnetlib.html>.
- [29] K. Binder and D.W. Heermann, Monte Carlo Simulation in Statistical Physics, (Springer-Verlag, 1992).
- [30] L. Devroye, Non-Uniform Random variate Generation, (Springer-Verlag, 1986).
- [31] A. Aharony and A.B. Harris, Phys. Rev. Lett. 77, 3700 (1996).
- [32] B. Efron, The Jackknife, the Bootstrap, and Other Resampling Plans (S.I.A.M., Philadelphia, 1982); B. Efron and R. Tibshirani, Statistical Science, vol. 1, 1986.

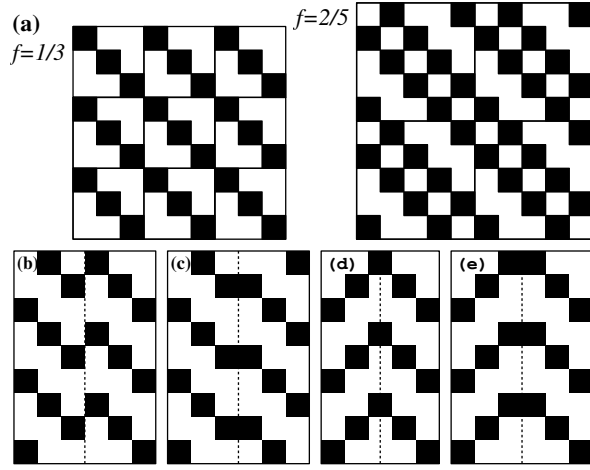


FIG. 1. (a) Fluxoid pattern for ground states of $f = \frac{1}{3}$ and $f = \frac{2}{5}$ (Unit cells are marked by solid lines). Domain wall fluxoid pattern for $f = \frac{1}{3}$: (b) shift-by-one wall, (c) shift-by-two wall, (d) herringbone wall, and (e) herringbone wall with a shift-by-two (a vortex is shown as a dark square).

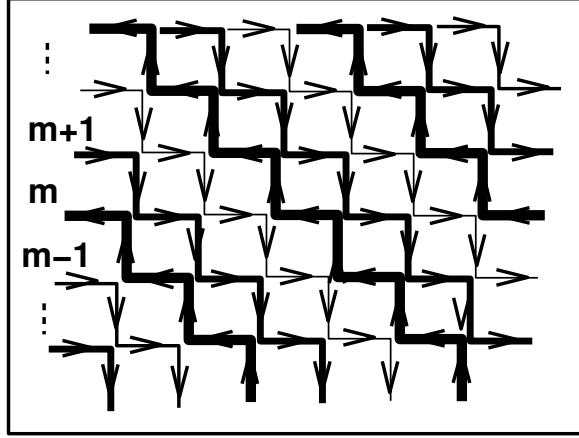


FIG. 2. Partition of the square lattice into staircases with the current flowing up or down the staircases.

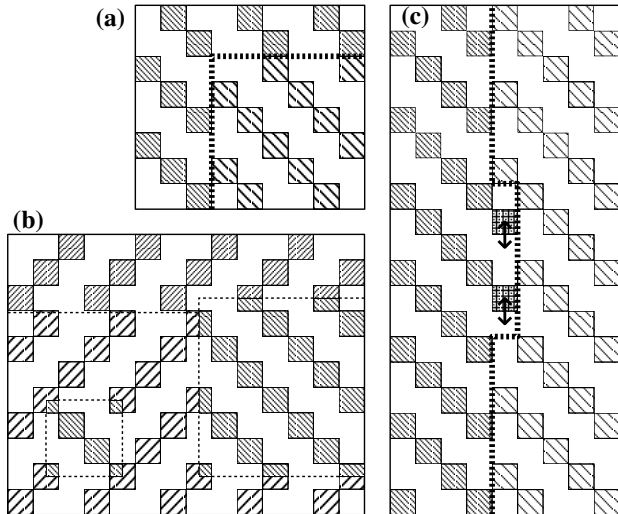


FIG. 3. Illustration of several possible bends and kinks in the different types of domain walls. (a) A 90 degree bend in a $f = \frac{1}{3}$ shift wall showing change from shift-by-one to shift-by-two wall. (b) $f = \frac{1}{3}$ shift-by-one wall branching into two herringbone walls. (c) Kink in a $f = \frac{1}{3}$ shift-by-three wall accomplished by moving the vortex marked in plaid.

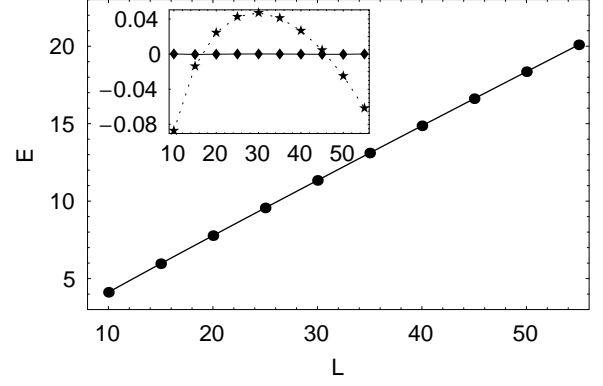


FIG. 4. Energy of a square domain of size $L \times L$ in a system with periodic boundary conditions of size 120×120 for $f = \frac{2}{5}$. The line is the fit $E = 0.0268(25) + 0.344797(68)L + 0.301(1) \ln L - 1.28(3)(L=120)^4$. The inset shows the residuals for a linear fit (stars) and the fit including the quadrupole corrections (diamonds).

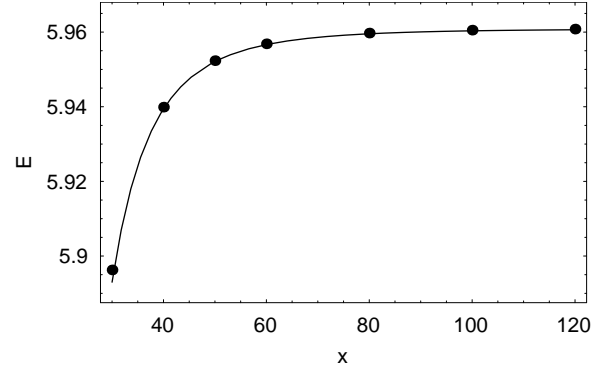


FIG. 5. Energy of a square domain of size 15×15 in a system with periodic boundary conditions of size $x \times x$ for $f = \frac{2}{5}$. The line is the fit $E = 5.961081(7) - 1.086(1)(15-x)^4$.

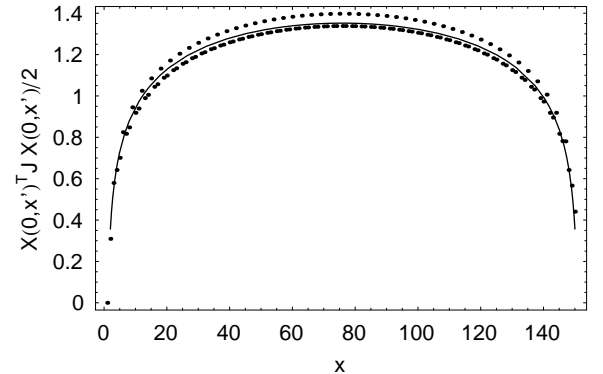


FIG. 6. $\frac{1}{2}X(x;x^0)^T J^{-1} X(x;x^0)$, the lattice "Green's" function, for $f = 1/3$ along a slice in the x -direction in a finite size system with periodic boundary conditions along the direction of the slice. The line indicates a fit to $A(\ln x + \ln(L-x))$.

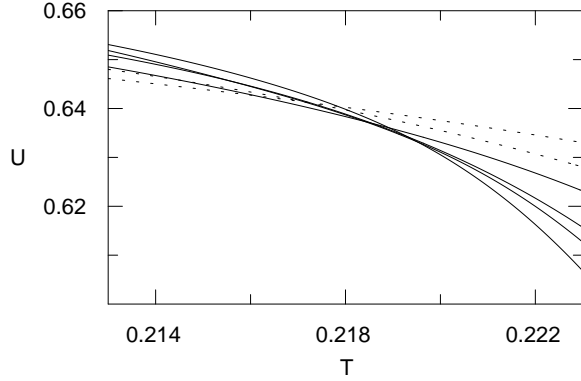


FIG. 7. $f = 1/3$ Binder's cumulant U vs T for $L = 36$ to $L = 84$ (smaller L shown as dotted lines).

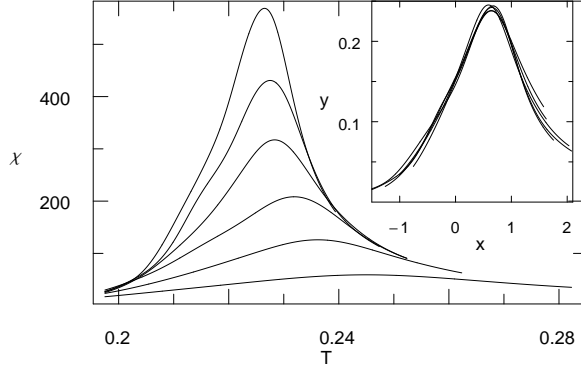


FIG. 8. $f = 1/3$ vs T for $L = 36$ to $L = 84$ and scaling collapse of this data (inset) where $x = (T - T_c)L^{1/\nu}$, $y = L^{-\beta/\nu}$, $\nu = 1$, and $\beta = \frac{7}{4}$.

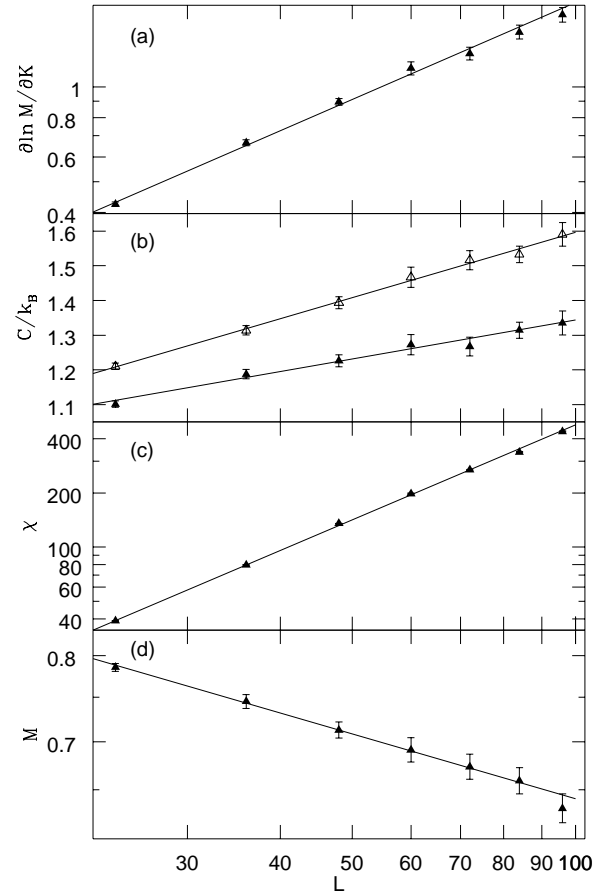


FIG. 9. Finite size scaling plots for $f = \frac{1}{3}$. (a) logarithmic derivative of M at T_c vs L , (b) specific heat maximum (hollow) and at T_c (solid) vs L , (c) χ at T_c vs L , and (d) M at T_c vs L .

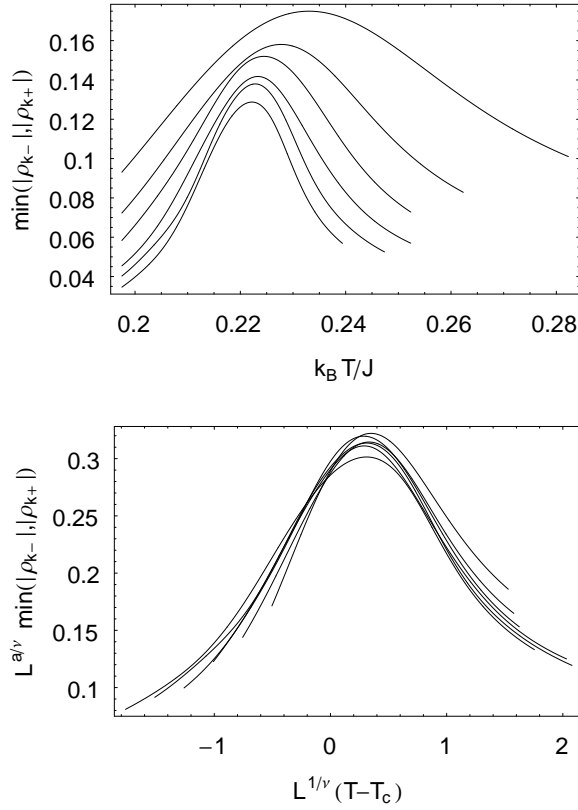


FIG. 10. $\min(|\rho_{k+}|, |\rho_{k-}|)$ versus $k_B T/J$. Note that data from larger L are smaller: $\min(|\rho_{k+}|, |\rho_{k-}|)$ vanishes as $L \rightarrow 1$ as indicated by the finite-size scaling plot (right) which shows a reasonable collapse for $\min(|\rho_{k+}|, |\rho_{k-}|) L^{a/\nu}$ with $a = 0.20 \pm 0.02$.

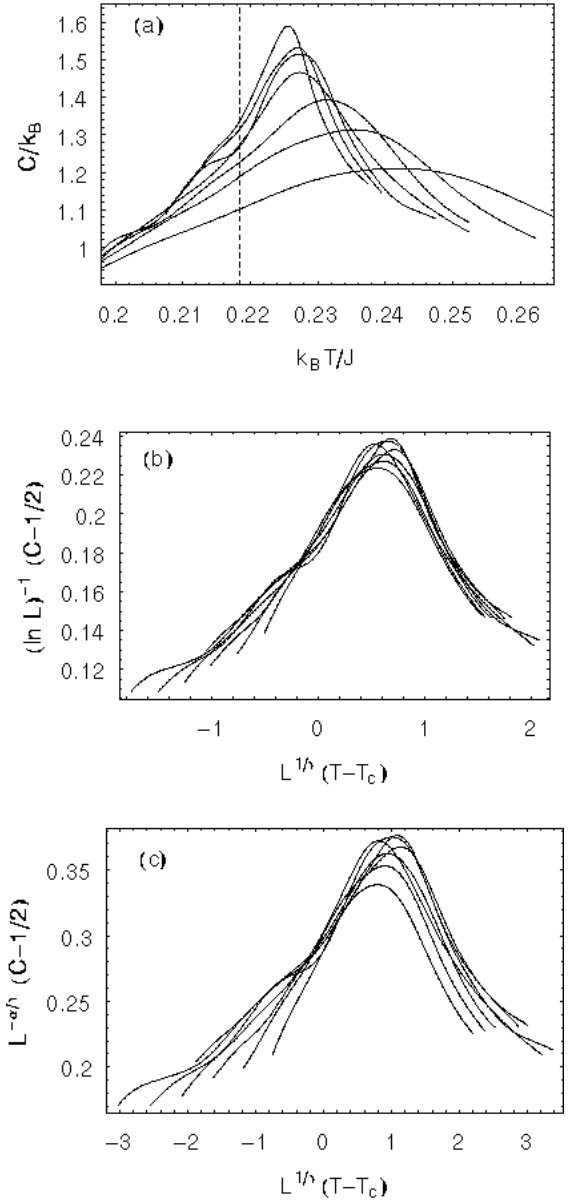


FIG. 11. (a) Specific heat for $L = 24$ to $L = 96$. The dashed line indicates T_c . Note that the shoulder which appears for intermediate lattice sizes goes away for the two largest L . This makes the scaling of C not as good as for the other variables. (b) Scaling collapse of data shown in (a). (c) Power law scaling found by Lee and Lee for smaller system sizes, applied to the data shown in (a). The logarithmic scaling shown in (b) gives a better collapse of the data. In particular the lower curve in (c), corresponding to the scaled $L = 96$ data is separating from the pack.

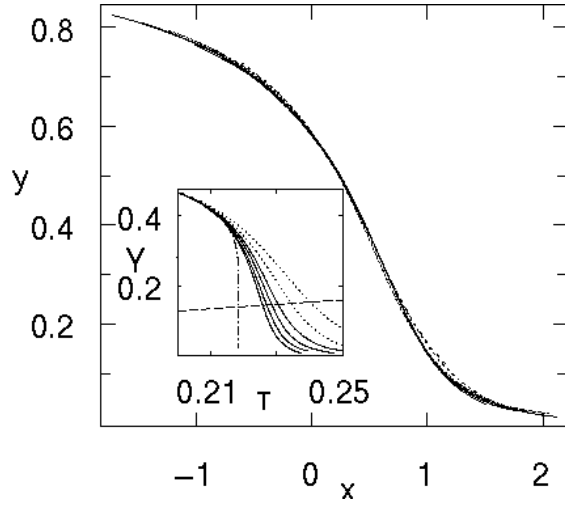


FIG. 12. Scaling collapse of Y where $x = (T - T_c)L^{1/\nu}$, $y = YL^{\beta/\nu}$, $\nu = 1$, and $\beta = \frac{1}{8}$. Inset: raw data (solid and dotted), T (dashed), and $a[T - T_c]$ (dot-dashed).

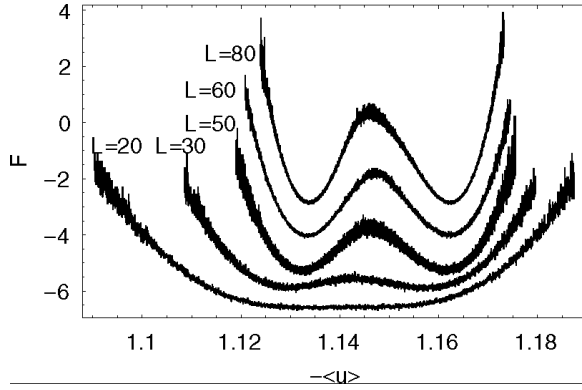


FIG. 13. Free energy as function of the negative of the energy per site for $f = \frac{2}{5}$ ($\nu = 0$). A constant has been added to the curves in order to separate them.

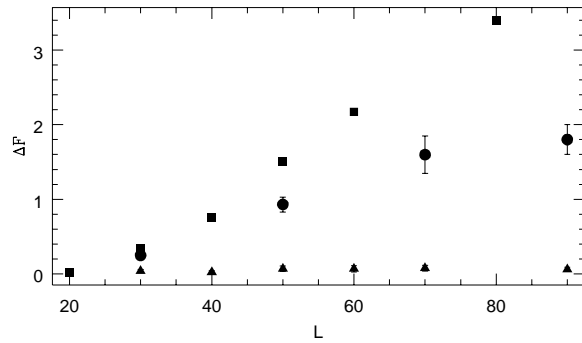


FIG. 14. Free energy barrier vs system size for $f = \frac{2}{5}$ and $\nu = 0$ (squares), 0.05 (circles) and 0.10 (triangles). ΔF is the bond disorder strength.

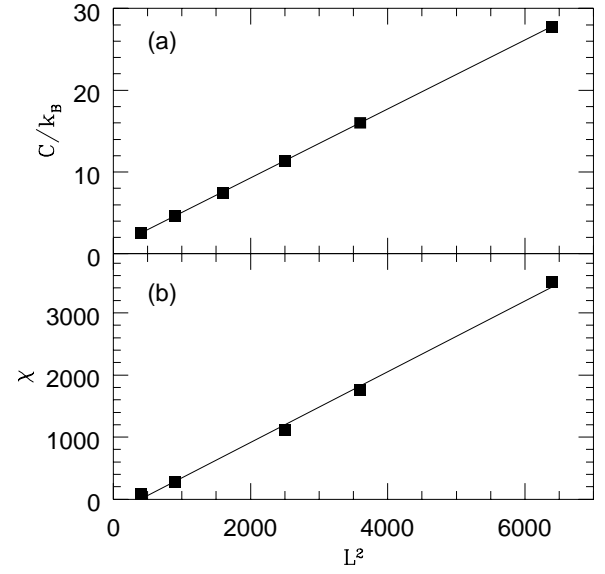


FIG. 15. (a) Specific heat versus L^2 and (b) susceptibility versus L^2 . Errors are comparable to the symbol sizes.

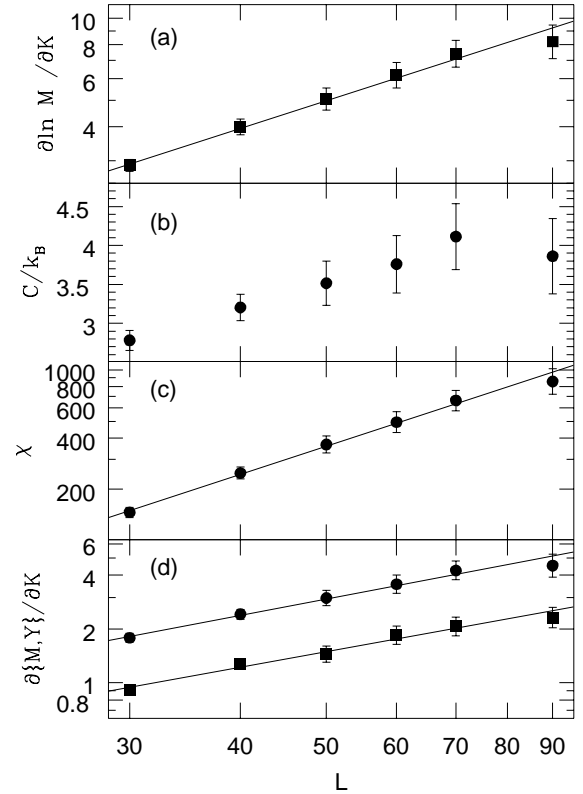


FIG. 16. Finite size scaling plots for $f = \frac{2}{5}$; $\nu = 0.1$: (a) logarithmic derivative of M vs L , (b) C/k_B vs L , (c) χ vs L , and (d) $@M=@K$ and $@Y=@K$ vs L

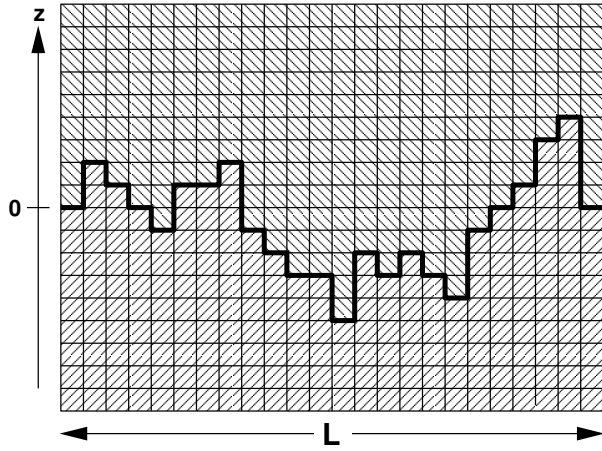


FIG. 17. Solid on solid interface. Overhangs and bubbles are ignored in the SOS model and interface configurations can be described in terms of integer-valued height variables measured from the straight, $T = 0$ configuration of the interface.

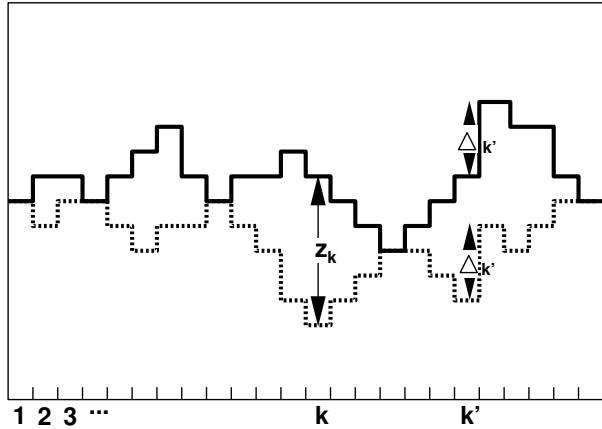


FIG. 18. Two solid on solid interfaces. The interfaces have a negative binding energy causing them to want to stick but they cannot cross. This "no crossing" condition results in an entropic repulsion which pushes the interfaces apart at high enough temperature. z_k is the separation of the interfaces at the k 'th step and ν_k is the number of steps the interfaces take in the same direction at the k 'th step.

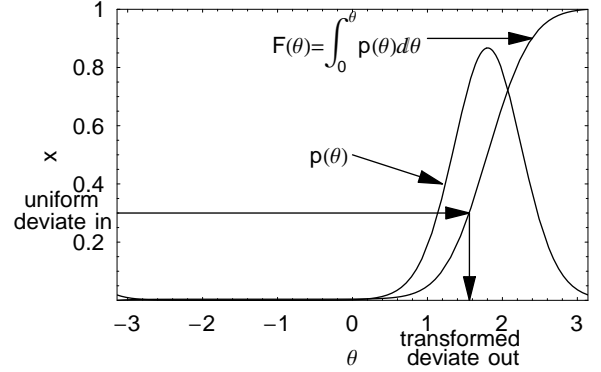


FIG. 19. Transformation method for converting a uniform deviate x into a random deviate distributed according to the function $p(\theta)$.

domain wall type	energy per unit length	
	$f = 1=3$	$f = 2=5$
herringbone-0	0:05673742 J	0:08611726 J
herringbone-1	0:19503538 J	—
shift-by-1	0:11419998 J	0:15889929 J
shift-by-2	0:16666667 J	0:16612232 J
shift-by-3	—	0:14764859 J

TABLE I. Domain wall energies for stable domain wall structures (i.e. walls which produce a vortex pattern consistent with $H_j = 0$ for every j). The n in herringbone- n denotes the associated shift where $n = 0$ is the standard herringbone.